

Robotic filament winding of advanced composite frames with complex geometrical shapes

Journal of Engineered Fibers and Fabrics

Volume 20: 1–18

© The Author(s) 2025

DOI: 10.1177/15589250241313157

journals.sagepub.com/home/jef

Jaroslav Mlýnek¹ , Seyed Saeid Rahimian Koloor² ,
Martina Rývolová³  and Tobias Dickhut² 

Abstract

Complex composite structure design is frequently practiced in today's aerospace and automotive industries. This study deals with the winding optimization of polymer composite frames having complex 3D geometry using rovings, winding heads, and industrial robots. This problem is addressed mainly from a geometrical perspective using a novel mathematical model and approach. Attention is given to maintaining the required winding angles, avoiding gaps, minimizing roving overlaps during winding, and ensuring the homogeneity of the windings process. Determination of the optimal number of rovings used and their width during the winding process is solved first for the case of a straight frame, where the central axis of the wound roving forms a straight helix on the frame surface. The winding technology for curved parts of the frame is more complicated. In practice, the curved section of the frame often forms geometrically part of a ring torus. The central axis of the wound roving then forms a toroidal helix on the torus. Optimization procedures are also solved for this type of frame. The verification of the derived theoretical conclusions was done using practical examples is a part of the research.

Keywords

Polymer composite frame, fiber winding, winding angle, ring torus, straight and toroidal helix, mathematical model

Date received: 9 August 2024; accepted: 28 December 2024

Introduction

Today, composite materials are increasingly used in developing and fabricating many products. They gradually replace conventional materials such as wood, steel, iron, and metal alloys.^{1,2} Its advantages include lightness, aggressive environment resistance, maintenance-free, tensile, flexural, and compressive strength.^{2,3} Recently, polymer composite frame applications have expanded. They are mainly used as reinforcements for aircraft wings and fuselages, landing gears, cabins, and doors of cars. Composite frames are also used to construct safety cab frames for off-road vehicles and agricultural machinery (e.g. tractors and harvesters), boats (hull reinforcements,

¹Department of Mathematics, Faculty of Science, Humanities and Education, Technical University of Liberec, Liberec, Czech Republic

²Chair of Composite Materials and Technical Mechanics, Institute of Aeronautical Engineering, Faculty of Mechanical Engineering, Universität der Bundeswehr München, Neubiberg, Munich, Germany

³Institute for Nanomaterials, Advanced Technologies and Innovation, Technical University of Liberec, Liberec, Czech Republic

Corresponding author:

Seyed Saeid Rahimian Koloor, Chair of Composite Materials and Engineering Mechanics, Institute of Aeronautical Engineering, Faculty of Mechanical Engineering, Universität der Bundeswehr München, Werner-Heisenberg-Weg 39, Neubiberg, Munich 85579, Germany.

Email: seyed.rahimian@unibw.de



Creative Commons CC BY: This article is distributed under the terms of the Creative Commons Attribution 4.0

License (<https://creativecommons.org/licenses/by/4.0/>) which permits any use, reproduction and distribution of the work without further permission provided the original work is attributed as specified on the SAGE and Open Access pages (<https://us.sagepub.com/en-us/nam/open-access-at-sage>).

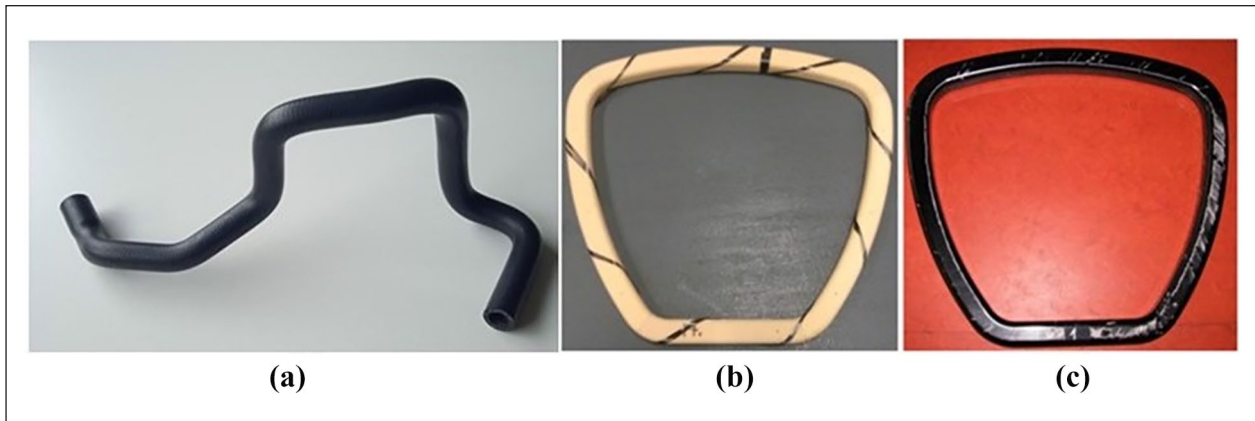


Figure 1. Frame shapes: (a) open composite frame of complicated shape, (b) closed frame with test winding of one roving, and (c) closed composite frame.

masts), and sporting goods, especially bicycles.^{1,4-6} Figure 1 shows examples of composite frames. They can be open (a) or closed (b), (c) and are often spatially constructed.

Figure 2 describes each step of the composite frame development process, while the individual steps are explained below in more detail.

Steps 1 and 2

Before starting the development of a composite frame, it is necessary to determine the shape and dimensions of the frame. Composite frames are often shaped only in 2D space. Determining the correct winding procedure is usually easier in such cases. In general, curved parts of frames shaped in 2D and 3D are the most difficult to wind. It is also necessary to define the requirements for the physical and mechanical properties of the future composite to ensure the composite frame's tensile, flexural, torsional, and compressive strength. Aggressive environment resistance with minimal maintenance is often essential to the composite requirements. A critical environmental aspect is the need for longer lifespans for composite frames and their recycling.

Step 3

The material composition and production technology are designed based on the specified requirements for the composite frame. The material composition includes:

- the type and properties of reinforcement (e.g. carbon, glass, basalt, aramid roving) and polymer matrix (thermosets, thermoplastic),
- number and orientation of layers,
- reinforcement preparation technology.

Three-dimensional or closed shapes require using a light-weight core, which has no significant effect on the final weight of the composite and its mechanical properties. Software modeling tools (e.g. Ansys, Abaqus) significantly assist in determining the components of composite and its mechanical properties.

Step 4

This step focuses on the issue of proper fiber winding on a composite frame from a geometric perspective and is the main focus of the article.

Step 5

The frame dry rovings reinforcement is then impregnated with resin and cured. Resin Transfer Molding (RTM) or vacuum infusion technologies are often used, depending on the resin type. The core (often from polyurethane foam) remains part of the finished composite.

Step 6

Followed by a comparison of the determined properties of the composite structure model (step 3) and the physical/measured values obtained by loading the composite component.

Steps 7 and 8

If the results of the practical tests of the composite prototype are in agreement, the technology for manufacturing the composite frame, including material composite composition, can be accepted. Otherwise, changes in previous Steps need to be made in the proposal, for example, in Step 3 when modeling the composite or material composition/composite structure in Step 2.

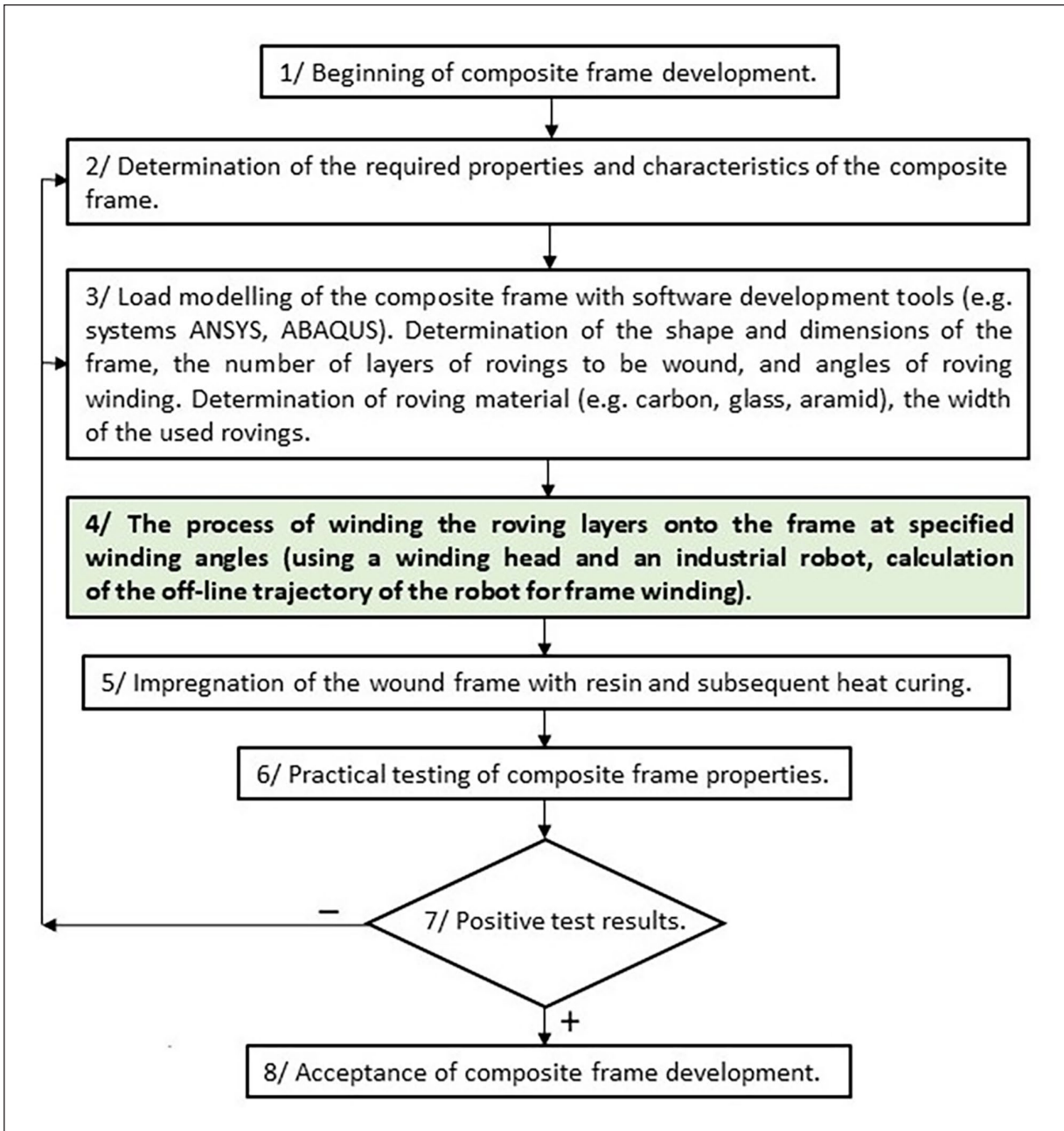


Figure 2. Schematic diagram of the composite frame development process.

Note 1

Roving is a fiber unit consisting of continual, unidirectional oriented filaments, usually without twists. Its cross-section has a lenticular shape.

The current research on mechanics of composite materials and structures mainly engaged on the issue of mechanical design at material and structural aspects, material characterizations,⁷ determination of mechanical behavior of composite structures at elastic to damage, and failure stages while considering structural response of composite

subjected to various loads,⁸ invention of high-performance materials with improve functionality for smart application and technology,⁹ engineering of materials for improving structural features within mechanical, thermal or even electrical features,¹⁰ etc. Within the mechanical-manufacturing aspects, the development of bio-based and biodegradable composites (lessen the environmental effect by traditional synthetic materials),^{11,12} structure with tailored properties at micro-to-meso level^{13,14}, 3D/4D printing within additive manufacturing techniques,^{15,16} etc. Experimental mechanics, assisted computational and

numerical techniques have been the most wrought methods accompanied to provide comprehensive insight for multidisciplinary study of composite and push the boundaries to create innovation and design based on complex industrial challenges.^{17–19} Although a lot of researches accomplished in these aspects, however there are plenty of aspects missing in the loop of manufacturing of complex composite structures including; defect formation at different material-levels for higher integration through compacting and layups,²⁰ guaranteeing uniform resin flow, and wetting to dense fibers,²¹ stable curing process and thermal control for optimum structural solidification,^{22,23} scalability of the structure considering the fabrication techniques, as well as incorporation of automation and robotics and quality control in the manufacturing processes.^{24,25} Emphasis in quality production of complex composite structures for aerospace applications was a the main basis in emerge of robotics and automation involvement in manufacturing of high-quality and high-performance structure pursued in research and development sectors of today's advanced industries.^{26,27} In this regard, robot winding is proven to be an effective method for quality production of curved composite frame, and recent researches has focused on optimization of winding processes. However, the problem of winding quality (winding angles, gaps reduction, or roving overlaps) is given much less attention in current research states. To solve this issue, the correct geometrical winding is essential to ensure the desired properties of the composite frame. For example, compliance with the prescribed angles of fiber layer orientation onto the frame is necessary to provide the composite's resistance to mechanical stresses.^{28–35}

The most common manufacturing processes for composite frames are braiding technology and filament winding. Two oppositely oriented layers from longitudinal textiles interlaced to crossing points characterize the braiding technology. The braided structure's benefit is the high adhesion of the fiber layer to the surface of the core or frame and the exact copy of the shape. Changes in cross-sectional shape or size are usually easy to solve by changing the feed rate. The core-feeding rate and trajectory shape are realized by using a robot.^{36–38}

In a commonly used procedure for filament winding technology, the frame core is rotated around its central axis. At the same time, the fibers are fed by a device attached to the robotic arm and moving parallel to the axis of the core. The angle of the filament winding depends on the speed of rotation of the frame core around the axis and the speed of movement of the filament feeder. The fibers are impregnated with resin before winding. Filament winding techniques are discussed, for example, in article,³⁹ and the advantages and disadvantages of using the winding technology are discussed in article.⁴⁰ Publication⁴¹ examines the conditions for maintaining the required winding angle.

The braiding technology and fiber winding procedures mentioned above are not applicable to the closed frame shape. The basis of the equipment for the production of braided structures is a ring with two rail lines for the opposing movement of the fiber carriers. Interference with the ring in terms of opening and closing it would be very complicated. For this reason, braiding machine manufacturers do not even offer a closed-core version of the braiding machine.

This paper focuses on a different winding technology of filament fibers on open- and closed-frame core types. Winding technology applies under certain conditions to frames with different cross-sectional shapes, such as circles, ellipses, triangles, or rectangles. The problem of winding rovings on a non-load-bearing frame of circular cross-section is solved in this article.

The winding head and industrial robot are used in the winding process. The frame is attached to the end of the robot's working arm (robot-end-effector), and, based on the suitable trajectory of the robot-end-effector, the frame gradually passes through the rotating rings of the winding head at a defined speed – a unidirectional fiber layers formed on the frame from coils located on the circumference of the rotating rings of the winding head (Figures 3(a), (b) and 4(a)). The setting of the size of the winding angle between the fiber layer and the frame axis is based on the assumption that the speed of the frame passage is constant and, at the same time, the variable angular velocity of the rotating ring (the robot's external axis controls the angular velocity of the rotating ring). The winding of two fiber rovings onto the frame as the frame passes through the winding head with two rotating rings is shown in Figure 3(b). A detail of the winding head is shown in Figure 3(c).

The rotating rings of the winding head are openable to allow winding of the closed frame core. Fiber rovings are wound dry only, wet winding cannot be used. The fibers are impregnated with resin after the winding process. To ensure the requested winding angle, it is also important, the central axis of the frame must be perpendicular to the plane of the rotating ring as the frame passes through the winding head. The rotate rings of winding head are composed of coils with fiber rovings (Figures 3(c), 4(a) and (b)). When passing the frame through a winding head with three winding rotating rings, the perpendicular position is approximated so that the individual winding angles are as close as possible to the desired value (deviation between the frame axis and the plane of the winding ring to be as close to 90° as possible). The problem of determining the optimized robot trajectory and ensuring the correct angle of roving winding for individual layers is described and solved in detail in the literature.^{1,42} Figure 4(b) shows the winding of the straight frame by carbon rovings and 4(c) combined winding with carbon and glass rovings.

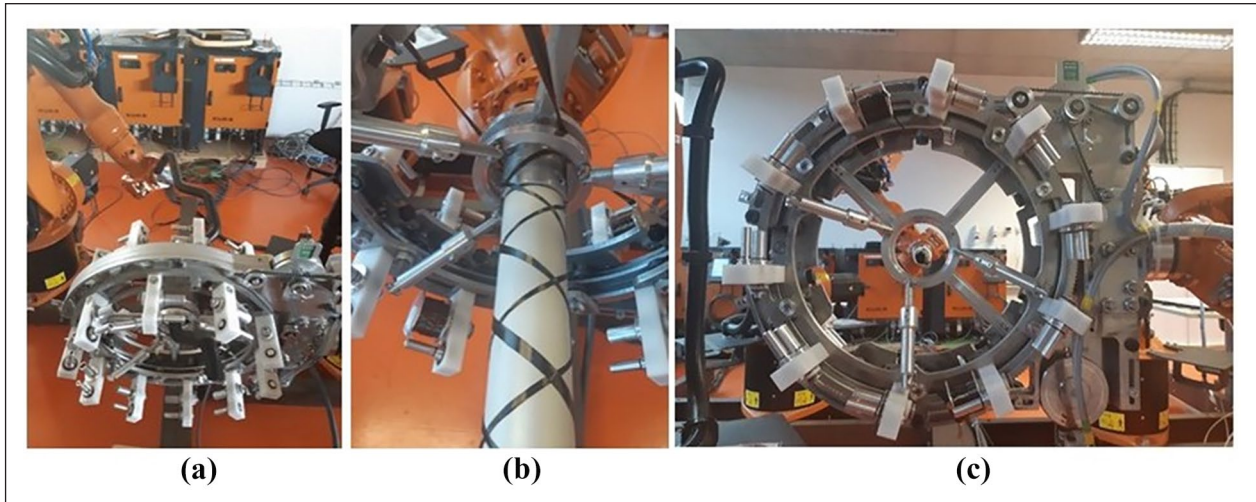


Figure 3. (a) Preparation of winding 2 layers of rovings on the frame attached to the robot-end-effector. (b) An example of winding only two carbon rovings on the frame is one at $+45^\circ$ and the other at -45° by two rotated ring of winding head. (c) Winding head with three rotating rings and spools.

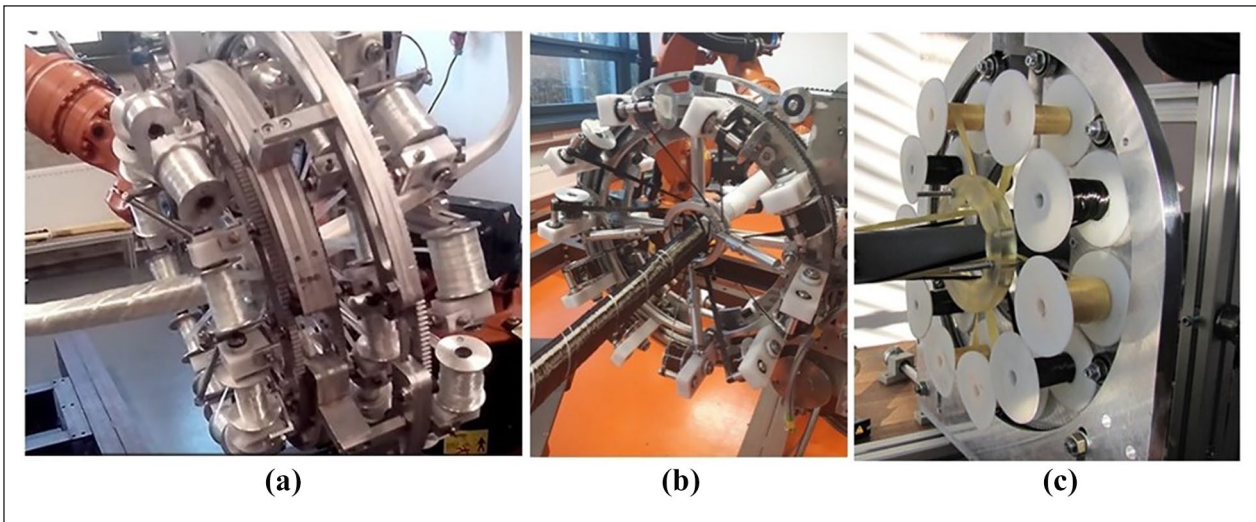


Figure 4. (a) Three rotating rings of winding head with glass rovings, (b) winding a straight frame with carbon rovings, and (c) combined winding with carbon and glass rovings.

The winding of a frame with two parts with different radii of cross-section is conditioned by a continuous transition between the parts (a truncated cone). The winding angle of fibers depends on the speed of passage of the frame through the winding head, the angular speed of rotation of the winding head ring and the frame radius. The speed of frame through the winding head is constant. To maintain the same winding angle on both parts of the frame, it is necessary to continuously change the angular speed of the rotating ring of the winding head (angular speed is controlled by the external axis of the robot). This issue is dealt with in detail in article.⁴

Material and methods

Achieving the required winding angle and roving windings without gaps and minimal overlaps is an important prerequisite for producing a quality composite frame. It is easier to meet these conditions when winding a straight frame with a circular cross-section. However, winding the curved parts of the frame is more difficult. The tendency to form gaps on the outer surface and large overlaps on the inner surface of frame arises when the curved part of the frame is wound. Also, the winding angle of the roving is greater on the outer surface than on the inner surface of the curved part of the frame.

The following two notes are important from the point of view of practical application of the presented results of this paper.

Note 2

As mentioned in Note 1, roving is a unit of filaments with lenticular cross-section. To simplify the mathematical model of winding the roving on the frame, we will further assume that the roving has a rectangular cross-section. In the mathematical model, only the width of the roving will be significant for the further derived procedures. The height of the roving is not solved in the model. These simplifications of the roving presentation do not affect the solution of the problems of the correct winding angle, gap formation, and overlap between two adjacent wound rovings. We examine only the geometric aspects of winding.

At the same time, we assume that when winding the roving onto the frame, the roving adheres to the frame along its entire length.

Note 3

The values of the roving width and the number of rovings used in winding the fiber layer are limited in the practical winding. The maximum number of rovings used is limited by the possible number of bobbins that can be attached to the rotating ring of the winding head. The width of the roving used is also limited by the offered range of roving manufacturers. However, knowledge the value of the overlap (gap) of two adjacent wound rovings is useful in selecting the appropriate roving width and the number of roving used.

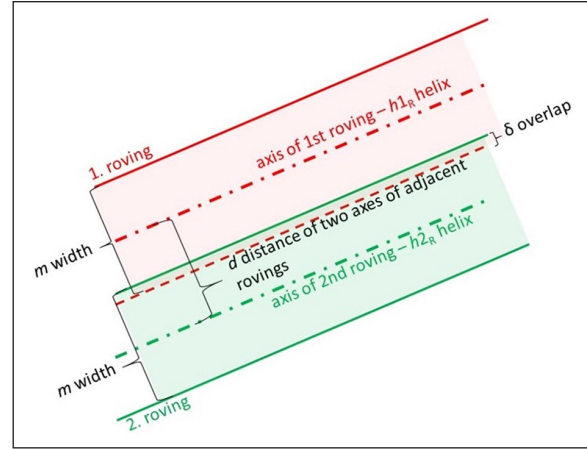


Figure 5. Display of two wound adjacent rovings (with marked central axes $h1_R$ and $h2_R$) unfolded into a plane.

Winding a straight frame

The central axis of the roving (see Figures 5 and 6(b)) forms a straight helix when the roving is wound onto a straight frame with a circular cross-section. A right-hand helix is formed when the winding angle is positive (denoted by +). Conversely, a left-handed helix is formed at a negative winding angle (denoted by -). The winding of one roving at an angle $+\frac{\pi}{4}$ ($+45^\circ$) and one roving at an angle $-\frac{\pi}{4}$ (-45°) on a straight frame of circular cross-section is shown in Figure 3(b). In the next part of the text, we will deal with the problem of a positive winding angle; the winding of a negative angle is analogous.

The parametric equation of right-handed helix h_R in a 3D Euclidean coordinate system can be expressed in the homogenous form⁴³:

$$h_R(t) = (x(t), y(t), z(t), 1) = (r \cdot \cos(t), r \cdot \sin(t), v_0(t), 1), \quad (1)$$

where v_0 is the reduced pitch of helix (length of translation of helix on $o \equiv z$ axis during rotation of the helix by 1 radian around o axis, $t \in <0, \infty$), see Figure 6(a). One turn of helix is defined by relation (1) for $t \in <0, 2\pi >$, A_1 is an initial point, and A_2 the final point of one turn of the helix, r is the radius of the frame, see Figure 6(a) and (b). The characteristics triangle of helix h_R with the definition of pitch, v is shown in Figure 6(a). The pitch v is defined as (see Figure 6(a) and (b))

$$v = \|A_1 A_2\| = \sqrt{\|h_R\|^2 - 4\pi^2 r^2}.$$

It can be seen that $\tan \alpha = \frac{v}{2\pi r}$ (Figure 6(a)), where α is the pitch angle of the helix (i.e. in our case, the

winding angle). The central axes $h1_R$ and $h2_R$ in Figure 7(a) of two adjacent wound rovings form right-handed helices. Both helices $h1_R$ and $h2_R$ have the same pitch angle α , $h2_R$ is rotated around the helix axis o (i.e. around the frame axis) relative to $h1_R$ by the angle λ .

Note 4

Composite and textile specialists often define β as a winding angle where

$$\beta = \frac{\pi}{2} - \alpha. \quad (2)$$

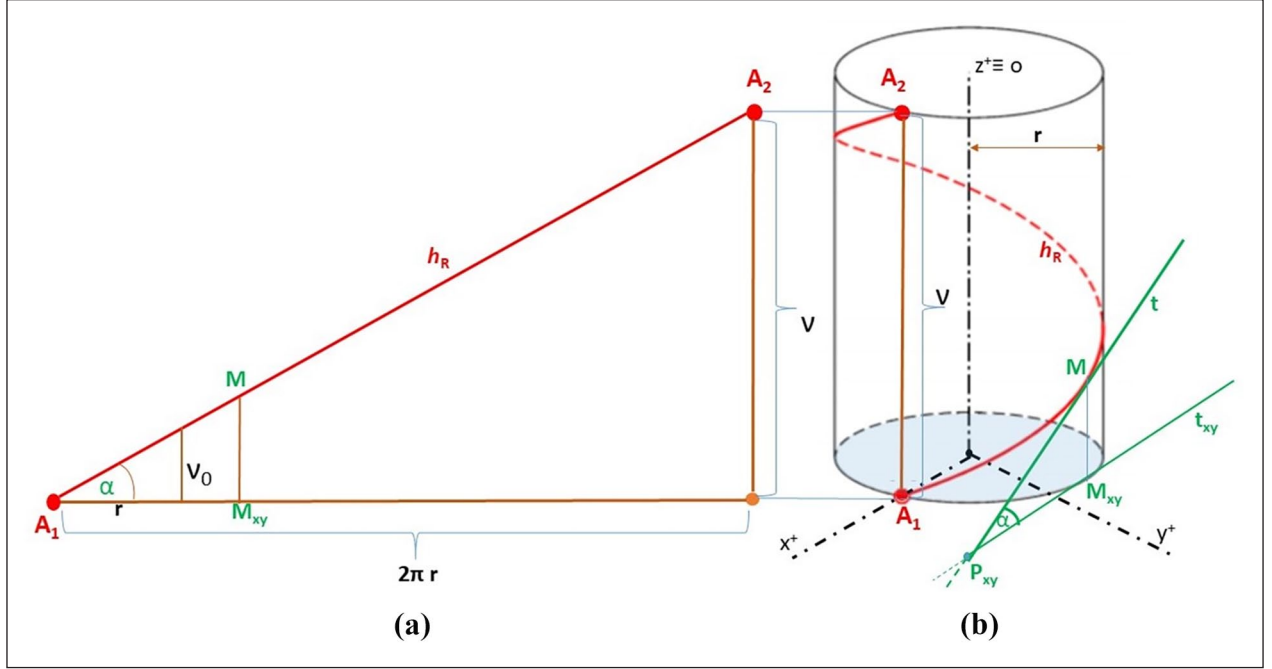


Figure 6. (a) Characteristic triangle of helix h_R . (b) One turn of the right-handed helix h_R , pitch of the helix v , helix pitch angle α .

In this article, the angle of the roving winding will be referred to as α angle.

Distance d of the central axes $h1_R$ and $h2_R$ of two adjacent wound rovings, width m of the roving, and ε_{str} overlap of adjacent wound rovings can be expressed in the form $m = d + \varepsilon_{str}$ (see Figure 5). At the same time, $d = \lambda r \sin \alpha$, see Figure 7(b). We remind that λ indicates the helix $h2_R$ rotation angle around axes o relative to helix $h1_R$ and r denotes the radius of the frame. From this follows ε_{str} overlap of two adjacent rovings is equal to

$$\varepsilon_{str} = m - \lambda r \sin \alpha. \quad (3)$$

It can be seen from relation (3) that the size of the ε_{str} overlap depends on the m width of the roving itself, angle λ , radius r of frame, and α winding angle.

We assume that the roving coils are evenly spaced around the circumference of the rotating ring of the winding head and the number of used coils is n . Then $\lambda = \frac{2\pi}{n}$ and from (3) implies

$$\varepsilon_{str} = m - \frac{2\pi}{n} r \sin \alpha. \quad (4)$$

Optimum m roving width can be expressed from relation (4) and setting overlap $\varepsilon_{str} = 0$.

Note 5

In the following, n number of rovings used will automatically be taken to include the number of coils used to wind the layer of rovings.

Optimum n number of rovings used in roving winding can be expressed from relation (4) and $\varepsilon_{str} = 0$ it follows

$n = \frac{2\pi}{m} r \sin \alpha$. Since the value of n represents the natural number of rovings used to wind the layer of rovings, it is necessary to modify the expression of the optimal number \tilde{n} to the form

$$\tilde{n} = \left\lceil \frac{2\pi r \sin \alpha}{m} \right\rceil. \quad (5)$$

The current corresponding overlap $\tilde{\varepsilon}_{str}$ is equal to

$$\tilde{\varepsilon}_{str} = m - \tilde{\lambda} r \sin \alpha = m - \frac{2\pi}{\tilde{n}} r \sin \alpha. \quad (6)$$

Note 6

The designation $\lceil x \rceil$ of a real number x is defined as $\lceil x \rceil = \min \{ p \in \mathbb{Z}; p \geq x \}$, where \mathbb{Z} denotes integer numbers.

The appropriate use of relation (4) can be used to express the required value of one of the parameters while knowing the remaining parameters. The procedures for determining the optimal number n of rovings used and the optimal roving width m are described in detail in Ref.⁴⁴

The ε_{str} overlap value in relation (4) meets one of the following three conditions.

1. If $\varepsilon_{str} < 0$ in relation (4), then during the winding process, there is a gap between two adjacent

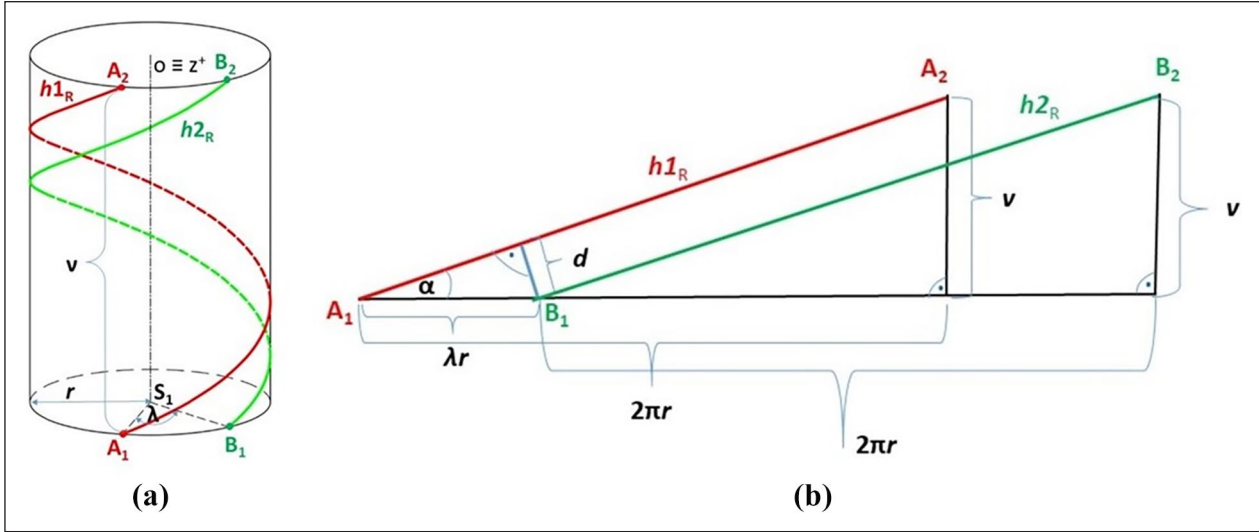


Figure 7. (a) One turn of helix h_{1R} and helix h_{2R} . Helix h_{2R} is rotated around the axis of the helix o concerning the helix h_{1R} by λ angle. (b) The unfolding of the cylindrical surface of h_{1R} and h_{2R} (one turn) into a plane.

rovings and the problem must be solved by increasing the number n of used rovings or use wider rovings (i.e. increase in the value of m).

- If $\varepsilon_{str} = 0$, then the theoretical ideal state occurs. The width m of the roving is the same as the distance d between the longitudinal axes (two axes h_{1R} and h_{2R} of two adjacent rovings in Figures 5 and 7(b)). Thus, no gap or overlap is created during winding. In practice, however, it is preferable if there is a small overlap (e.g. $\varepsilon_{str} = 1$ mm).
- If $\varepsilon_{str} > 0$, then there is no gap in the winding of adjacent rovings, and ε_{str} -sized overlap is created. In this case, it is necessary to consider whether width ε_{str} overlap is acceptable in terms of the winding's quality.

Winding a curved frame

Winding rovings on the curved frame is more difficult than the straight part. The same winding angle cannot be achieved over the entire surface of the curved part of the frame. Generally, the winding angle is greater on the outer curved part of the frame surface than on the inner part. If the bending of the frame is realized with a small radius and a large angle of curvature, then it is technically difficult to realize the winding of the rovings and to ensure an acceptable deviation of the required winding angle. As a last resort, it is necessary not to wind the frame and to design a different geometry for the composite frame. The curve of the frame part can be realized in 2D or 3D. Winding a 3D curved frame section is generally more complicated than a 2D curve.

Winding a torus-shaped frame section. In practice, a curved section of a frame often creates a geometric part of a ring

torus that is a rotating surface in 3D. However, the ring torus curvature is only implemented in 2D. It is formed by rotating a circle k with radius r and center K about an axis o lying in the plane of the circle k at a distance R from the center S (see Figure 8(a)).

The ring torus can be expressed parametrically in 3D right-handed Euclidean space in the form (see Ref.⁴⁵ p. 65)

$$x(\theta, \varphi) = (R + r \cos \theta) \cos \varphi,$$

$$y(\theta, \varphi) = (R + r \cos \theta) \sin \varphi,$$

$$z(\theta, \varphi) = r \sin \theta. \quad (7)$$

The major radius R denotes the distance of the point K from the central axis o (see Figure 8(a)). Point K is the center of the rotating circle k with minor radius r . Angles θ and φ take values from the interval $<0, 2\pi$). Angle θ ensures rotation around point K with radius r (circle k), whereas φ represents rotation circle k around axis o .

The *aspect ratio* a of ring, torus is defined as (see Ref.⁴⁵)

$$a = \frac{r}{R}. \quad (8)$$

The parameter a defined by relation (8) characterizes the difficulty of winding the roving on the ring torus. The closer the value of a is to zero, the better the conditions for quality roving winding.

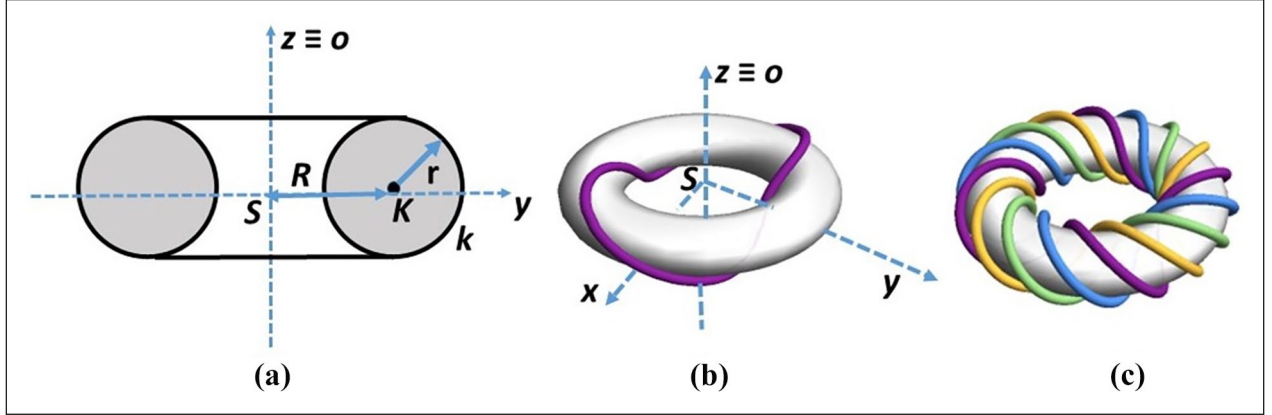


Figure 8. (a) Description of the ring torus – used to define the rotation surface geometrically. (b) Two turns ($\omega = 2$) of toroidal helix on ring torus. (c) Four turns ($\omega = 4$) of four toroidal helices on the ring torus.

The parametric expression of a right-handed *toroidal helix* (see Figure 8(b)) can be expressed in the form (see Ref.⁴⁶)

$$\begin{aligned} x(t) &= (R + r \cos(\omega t)) \cos t, \\ y(t) &= (R + r \cos(\omega t)) \sin t, \\ z(t) &= r \sin(\omega t). \end{aligned} \quad (9)$$

The parameters R and r have the same meaning as in relation (7). Parameter $t \in R$ and ω is a real positive number. Relation (9) describes the winding toroidal helix on the ring torus surface defined by relation (7). If ω is a natural number, it indicates the number of turns of the toroidal helix on the ring torus. *Toroidal pitch* H specifies the length of repetition along the central axis o of the ring torus (see Figure 9(a)) and is defined by the relation (see Ref.⁴⁶):

$$H = \frac{2\pi R}{\omega}. \quad (10)$$

The central axis o of the torus (see Figure 9(a)) passes through the winding head at the same speed as the central axis o of the straight frame during winding (see Figure 6(b)). Recall that v denotes the pitch of the helix and α desired winding angle. Then based on Figure 6(a) it implies

$$H = v = 2\pi r \operatorname{tg} \alpha. \quad (11)$$

From relations (10) and (11) it follows

$$\omega = \frac{2\pi R}{2\pi r \operatorname{tg} \alpha} = \frac{R}{r \operatorname{tg} \alpha}. \quad (12)$$

The relation (12) defines the ω parameter for equation (9) of parametric expression of the toroidal helix. In the parametric expression of the toroidal helix (9), the ω parameter replaces α winding angle. As the value of ω increases, the number of turns of h_R axis roving around the torus increases, and thus, the winding angle decreases.

The required α angle of the roving winding on the frame can only be achieved on a straight frame. When winding the roving on the ring torus, the largest winding $\tilde{\alpha}_{ext}$ angle occurs on the outer circle p_1 and the smallest $\tilde{\alpha}_{int}$ on the inner circle p_2 (see Figure 9(a)) For $\tilde{\alpha}$ winding angles on the remaining area of the ring torus, the relation holds $\tilde{\alpha}_{int} < \tilde{\alpha} < \tilde{\alpha}_{ext}$. At the same time $\tilde{\alpha}_{int} < \alpha < \tilde{\alpha}_{ext}$, where α is the desired winding angle. The issue of winding angle is discussed in detail in Ref.⁴⁷

The arc length part l_{02} (with endpoints T_0 and T_2) of one rotation of h_R axis on the outer p_1 circle (see Figure 9(a)) is equal to (see Ref.,⁴⁸ p. 11) $l_{02} = \frac{2\pi}{\omega}(R+r)$ and analogously arc length part l_{13} (with endpoints T_1 and T_3) of one rotation of h_R axis on the inner circle is equal to $l_{13} = \frac{2\pi}{\omega}(R-r)$. The placement of the roving on the part of the outer circle p_1 is shown in Figure 9(b).

Let us assign the following values to δ_0 and δ_1 singles

$$\begin{aligned} \delta_0 &= \arccos \left(\frac{R+r}{\sqrt{(R+r)^2 + r^2 \omega^2}} \right), \\ \delta_1 &= \arccos \left(\frac{R-r}{\sqrt{(R-r)^2 + r^2 \omega^2}} \right) \end{aligned}$$

and as well as c_0 , c_1 parameters $c_0 = m / \sin \delta_0$ and $c_1 = m / \sin \delta_1$.

In article,⁴⁷ it is shown in detail that the ε_{out} overlap of two adjacent rovings on the outer circle p_1 and ε_{inn}

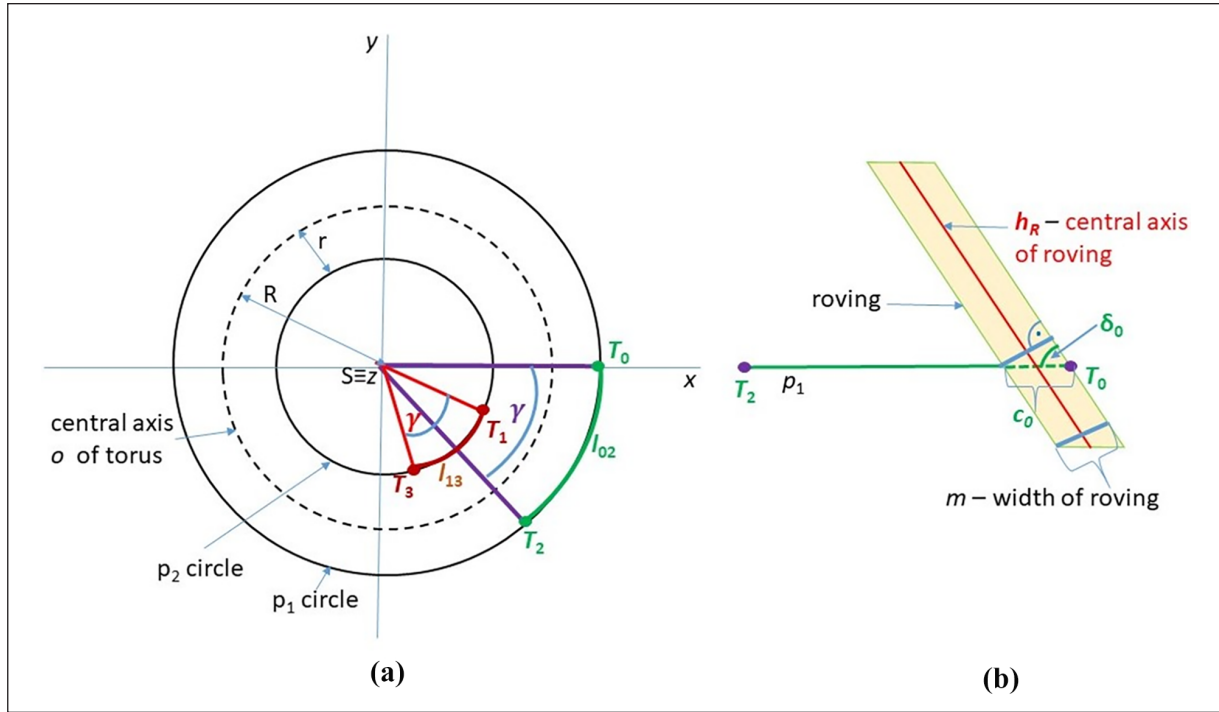


Figure 9. (a) Floor plan of ring torus; o – central axis of the ring torus, p_1 – circle on the outer surface of the ring torus, p_2 – circle on the inner surface of the ring torus, arc length part l_{02} – one period distance of toroidal helix on the outer circle p_1 , arc length part l_{13} – one period distance of toroidal helix on the inner circle p_2 . (b) Laying a roving of width m on part l_{02} of outer circle p_1 .

overlap of two adjacent rovings on the inner circle p_2 of the torus are equal to

$$\varepsilon_{out} = \frac{n \cdot c_0 - l_{02}}{n}, \quad \varepsilon_{inn} = \frac{n \cdot c_1 - l_{13}}{n}. \quad (13)$$

For a given number of used rovings n and their width m , the size of overlaps ε_{out} and ε_{inn} of two adjacent wound rovings on the outer p_1 circumference and inner p_2 circumference of the torus can be calculated using relation (13). In general, the relation $\varepsilon_{out} < \varepsilon_{inn}$ is true, that is, the overlap on p_1 the outer circuit is always smaller than on p_2 inner circuit.

The ε_{out} overlap value in relation (13) meets one of the following three conditions.

1. If $\varepsilon_{out} < 0$, then a gap is created between two adjacent wound rovings on the outer circumference p_1 of the torus. From the point of view of the quality of roving winding, such a situation is unacceptable. It is necessary to use a larger number n of rovings or rovings with a larger width m .
2. If $\varepsilon_{out} = 0$, the windings of adjacent rovings build on each other and are without overlap, which is the ideal state. At the same time, it is necessary to

calculate the value of ε_{inn} , which gives the overlap of adjacent rovings on the inner circumference p_2 . When it holds for a aspect ratio (see relation (8)) $a \rightarrow 1$, there may be an unacceptable overlap of two adjacent rovings on the inner circumference of p_2 . The use of more n number of rovings with smaller width m is required.

3. If $\varepsilon_{out} > 0$, it is necessary to assess whether ε_{out} and ε_{inn} overlaps are acceptable.

For the given ring torus, toroidal helix parameters, and fixed n number of rovings used in the winding of a layer on a curved section of a torus-shaped frame, the optimal width m of the roving is derived in Ref.⁴⁷ The optimum width m is then determined by the relation

$$m = \frac{2\pi}{\omega n} \cdot (R + r) \cdot \sin \delta_0. \quad (14)$$

For optimal m width of the roving determined by relation (14), $\varepsilon_{out} = 0$ and the value of ε_{inn} should be calculated according to relation (13).

Similarly, for the given roving width m , the optimal number \tilde{n} of rovings used in the layer winding is derived in detail in an article⁴⁷ and is expressed by the relation

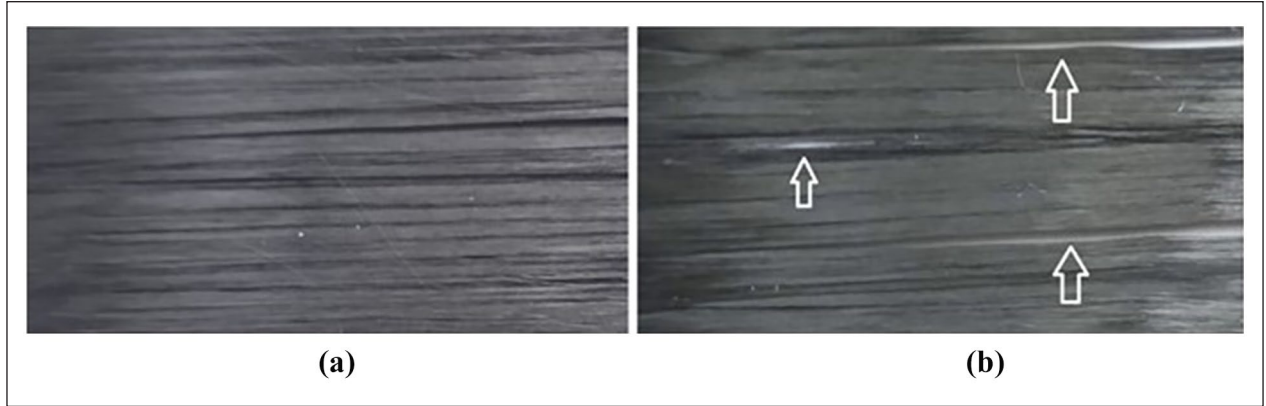


Figure 10. Carbon fiber reinforced layers; (a) Homogenous fiber distribution. (b) Layer with gaps (marked by arrows).

$$\tilde{n} = \frac{2\pi}{\omega \cdot m} \cdot (R + r) \cdot \sin \delta_0. \quad (15)$$

It is then convenient to calculate overlaps ε_{out} and ε_{inn} in relation (13) for a given \tilde{n} by equation (15).

Based on the derived relations in paragraphs 2.1. and 2.2. the following calculations can be performed for a frame with a straight section and a section created by part of the ring torus. Specified parameters are the following: r – radius of frame, R – major radius of frame section that forms part of ring torus and required α winding angle.

Straight section of the frame

1. Entered: number of n rovings used, m width of rovings.

The ε_{str} overlap of two adjacent rovings can be determined by relation (4).

2. Determining m optimal width of the rovings for a given number n of rovings used and setting ε_{str} overlap of two adjacent rovings $\varepsilon_{str} = 0$ in relation (4).
3. Determination of \tilde{n} optimal number of rovings used for a given m roving width by relation (5) and calculation of corresponding $\tilde{\varepsilon}_{str}$ overlap by relation (6).

Torus-shaped frame section

1. 1/ Entered: n number of roving used, m width of rovings.

The ε_{out} and ε_{inn} overlaps of two adjacent rovings on the outer p_1 and inner p_2 circles of torus can be determined by relation (13). If $\varepsilon_{out} < 0$, then a gap is created between two adjacent wound rovings on the outer circle p_1 of the torus, and such a situation is unacceptable.

2. Determining m optimal width for a given number n of rovings used relation (15). Performing the calculation of ε_{inn} by relation (13).
3. The m width of the roving is specified, and the calculation of the optimal \tilde{n} number of used rovings by relation (14). Then, calculate overlaps ε_{out} and ε_{inn} using relation (13).

The optimized winding of the rovings on the frame is based on the following principle⁴⁹:

- (A) the winding of the frame must not contain a gap,
- (B) overlaps of adjacent rovings should be minimal.

Compliance with condition (A) has a higher priority than condition (B).

Based on the above principles, it is suitable to select the appropriate width m and number n of rovings to be used together on all parts of the frame. Since the winding of the rovings on the frame is continuous, selecting the number of rovings to be used and their width is necessary so that conditions (A) and (B) are satisfied.

Result and discussion

This section focuses on practical examples of using the derived relations in Chapter 2. Attention will be focused on determining the optimal width of the wound rovings, the optimal number of rovings used during winding, and the possible gaps (Figure 10) and overlapping rovings resulting from winding adjacent rovings.⁴⁹ The vertical cross-section of all frames referred to in this chapter is circular. The calculation will be carried out successively for a straight frame, a ring torus frame, and a frame composed of two straight arms connected by a quarter-torus part.

An enlarged image of the roving winding on the frame is shown in Figure 10. Subfigure (a) contains a homogenous winding, while subfigure (b) contains gaps.

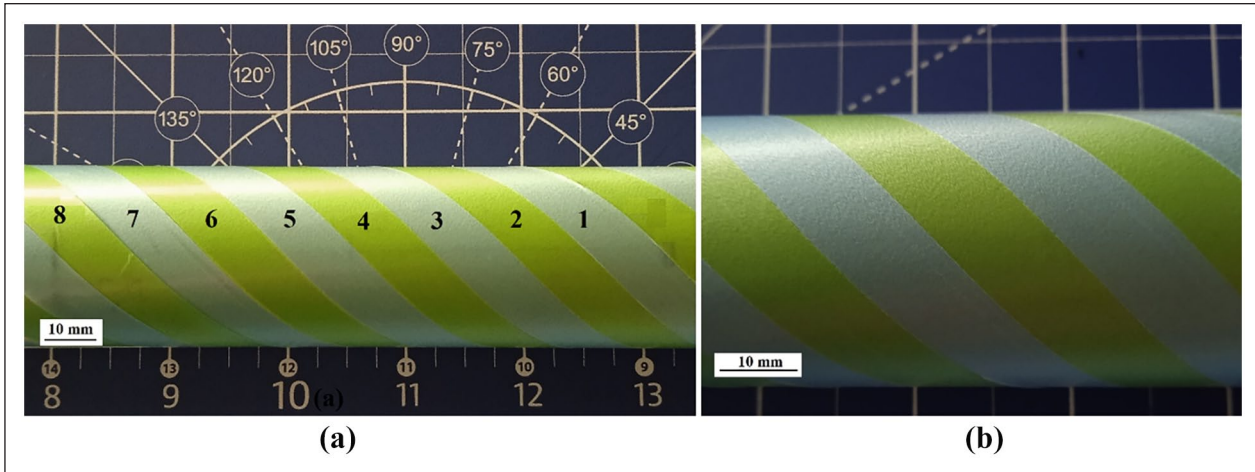


Figure 11. (a) Winding a layer of eight rovings/tapes on a straight frame (corresponding to the following input values of Table 1: radius of frame $r=18$ [mm], $n=8$, $\alpha=45^\circ$). Overlapping adjacent rovings/tapes is zero ($\varepsilon_{str}=0$). (b) Detail of wound rovings/tapes.

Note 7.

The width of the roving primarily depends on the number of used filaments. The most frequently used rovings for winding technology are 24K (24,000 fibers, 9–10[mm] width) and roving 12K (12,000 fibers, 5–6[mm] wide). Roving filaments of 6K (6000 fibers) or 3K (3000 fibers) are arranged in strands and are more suitable for braiding technology.

Note 8.

Figures 11 to 15 are photographs of real windings. In accordance with Notes 2 and 3, the winding was done with green and blue tapes (to color distinguish adjacent tapes) with a rectangular cross-section. Therefore, when using color tapes, the following is indicated as “roving/tape.” The conclusions drawn from the tests and concerning the winding angles, gaps and overlaps of adjacent wound strips are the same as for the rovings with lenticular cross-section.

Example 1 – straight frame

As mentioned, when winding a frame with a circular cross-section, the rovings can be wound at the desired α angle. Let entered radius r of the frame and the winding angle α ; the following types of calculations can be performed.

1. Width m of the roving and the number n of rovings during the winding of the layer is determined, using relation (4) to the calculation of size ε_{str} of the overlap of two adjacent.
2. It is defined n number of rovings used during winding, and it requires zero overlaps of two

adjacent rovings (i.e. $\varepsilon_{str}=0$), using relation (4) can be determined the optimal width m of the roving.

3. It is fixed m width of roving and the optimal number n of for roving can be calculated using relation (5), and corresponding $\tilde{\varepsilon}_{str}$ overlap is determined by (6).

The winding of a fixed number n of rovings with the optimum calculated width m of roving for angles $\alpha=30^\circ, 45^\circ$, and 60° is shown in Table 1. The ε_{str} overlap of adjacent rovings is zero ($\varepsilon_{str}=0$) for the optimal m roving width. Figure 11 shows the winding of rovings/tapes on a straight frame corresponding to the second row of Table 1.

Table 2 contains calculations of the optimal \tilde{n} number of rovings used to wind and overlap $\tilde{\varepsilon}_{str}$ for the specified roving m width.

Figures 12 and 13 show the winding of rovings/tapes on a straight frame corresponding to the fourth and fifth rows of Table 2.

Example 2 – closed frame – ring torus

The winding of rovings on the curved frame of the ring torus part is solved in this example. For simplicity, the entire ring torus is considered in the example. Let the values R and r of the ring torus and the desired winding angle α be specified. The following types of calculations are possible to perform.

1. The m width of the roving and the n number of rovings used are specified. Calculate the overlaps of adjacent rovings on the outer circle p_1 (overlap ε_{out})

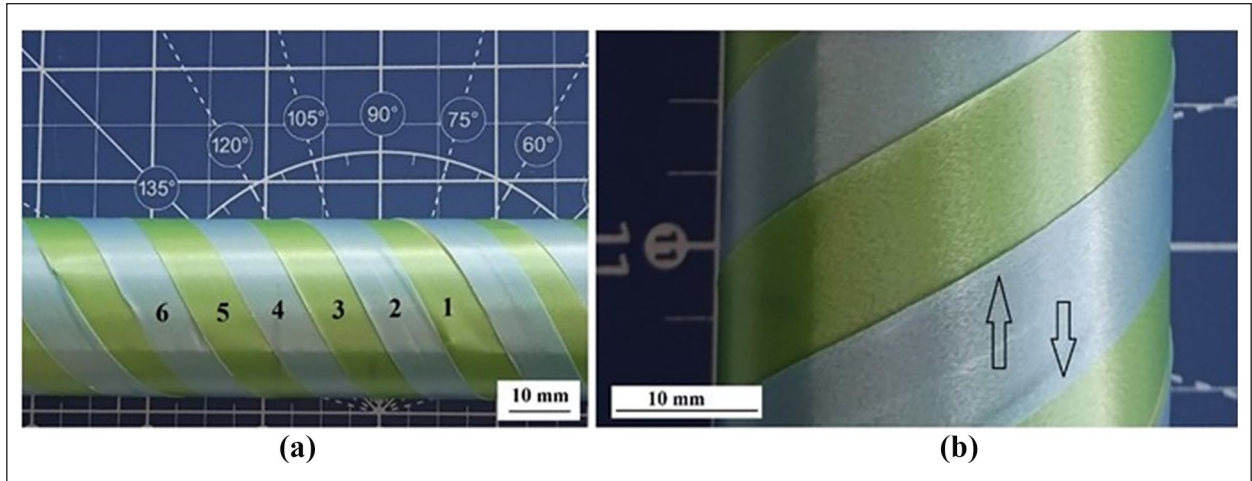


Figure 12. (a) Winding a layer of rovings/tapes on a straight frame (corresponding to the following input values of Table 2: radius of frame $r = 18[mm]$, $m = 10[mm]$, $\alpha = 30^\circ$). Overlapping $\tilde{\varepsilon}_{str}$ of adjacent rovings/tapes is small. (b) Enlarged view of wound rovings/tapes with negligible overlaps marked.

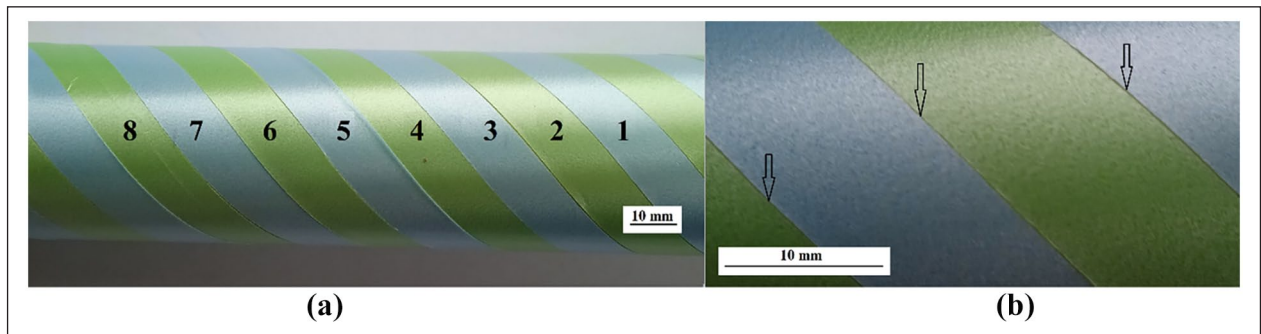


Figure 13. (a) Winding a layer of rovings/tapes on a straight frame (corresponding to the following input values of Table 2: radius of frame $r = 18[mm]$, $m = 10[mm]$, $\alpha = 45^\circ$). Overlapping $\tilde{\varepsilon}_{str}$ of adjacent rovings/tapes is negligible. (b) Enlarged view of wound rovings/tapes with negligible overlaps.

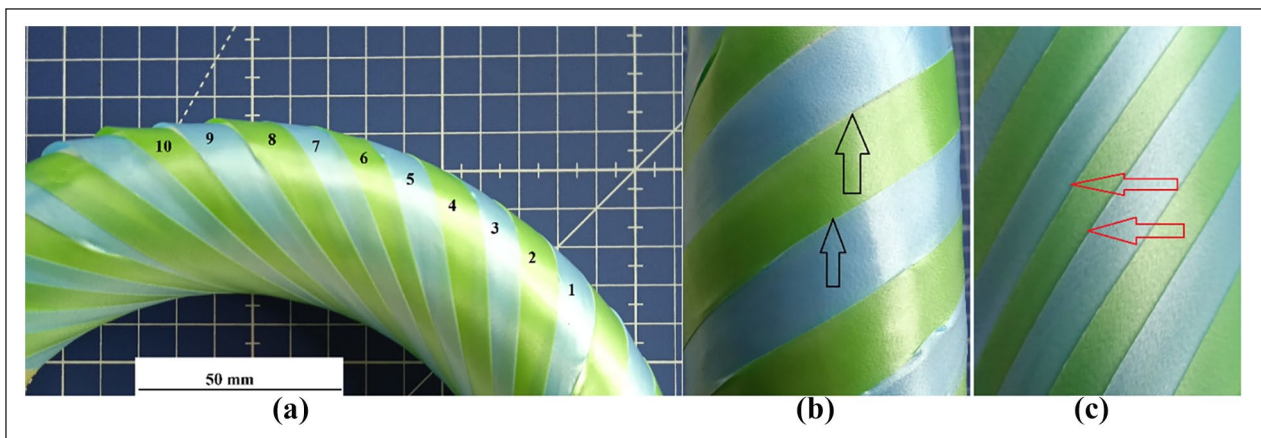


Figure 14. (a) Winding a layer of rovings/tapes on a toroid-shaped frame (corresponding to the following row input values of Table 4: major radius of torus $R = 90[mm]$, minor radius $r = 19[mm]$, $m = 10[mm]$, $\alpha = 45^\circ$). (b) Enlarged view on outer surface (circle p_1 , see Figure 9(a), marking of overlaps). (c) Enlarged view on the inner surface (circle p_2 , see Figure 9(a), marking of overlaps).



Figure 15. Winding a layer of rovings/tapes on a shaped frame (input values correspond to Table 5: major radius of torus $R = 102[mm]$, minor radius $r = 18[mm]$, winding angle $\alpha = 45^\circ$). (a) Several rovings/tapes according to parameters of the toroidal part (nine, Table 5), (b) Detail of overlaps on the toroidal part.

Table 1. Calculation of the optimal m roving width at zero overlap of adjacent wound rovings (when $\varepsilon_{str} = 0$).

Input parameters			Output parameter	
Radius(r) [mm]	Number of rovings (n)	Winding angle (α) [°] [rad]		Optimal width of roving (m) [mm]
18	8	30	0.5235	7.0085
		45	0.7853	9.9963
		60	1.0471	12.2430
36	12	30	0.5235	9.4247
		45	0.7856	13.3284
		60	1.0471	16.3235

Table 2. Calculation of the optimal \tilde{n} number of used rovings, and overlap $\tilde{\varepsilon}_{str}$ of adjacent rovings for a fixed roving m width.

Input parameters			Output parameter		
Radius (r) [mm]	Width of roving (m) [mm]	Winding angle (α) [°] [rad]		Optimal number of rovings (\tilde{n})	Roving overlap ($\tilde{\varepsilon}_{str}$) [mm]
9	6	30	0.5235	5	0.3451
		45	0.7853	7	0.2877
		60	1.0471	9	0.5586
18	10	30	0.5235	6	0.5752
		45	0.7853	8	0.0035
		60	1.0471	10	0.2054
36	14	30	0.5235	9	1.4336
		45	0.7856	12	0.6713
		60	1.0471	14	0.0078

Table 3. Calculation of the optimal m roving with zero overlap at the external circle p_1 of adjacent wound rovings ($\varepsilon_{out} = 0$). Parameter ω is calculated by relation (12).

Input parameters					Output parameters	
Major radius (R) [mm]	Minor radius (r) [mm]	Number of rovings (n)	Winding angle (α) [°]	Param. ω (ω)	Optimal width of roving (m) [mm]	Internal overlap (ε_{inn}) [mm]
90	19	8	30	8.2044	8.5513	2.6005
			45	4.7368	11.5228	2.9067
			60	2.7348	13.4713	2.4200
		12	30	8.2044	5.7008	1.7333
			45	4.7368	7.6687	1.9199
			60	2.7348	8.9792	1.6105

Table 4. Determination of optimal number \tilde{n} of rovings with width m . Calculations overlap $\tilde{\varepsilon}_{out}$ and overlap $\tilde{\varepsilon}_{inn}$. Parameter ω is calculated by relation (12).

Input parameters					Output parameters		
Major radius (R) [mm]	Minor radius (r) [mm]	Width of rovings (m) [mm]	Winding angle (α) [°]	Param. ω (ω)	Optimal number of roving (\tilde{n})	External overlap ($\tilde{\varepsilon}_{out}$) [mm]	Internal overlap ($\tilde{\varepsilon}_{inn}$) [mm]
90	19	6	30	8.2044	12	0.3649	2.0618
			45	4.7368	16	0.8374	1.7577
			60	2.7348	18	0.0279	1.0971
		10	30	8.2044	7	0.2837	3.2206
			45	4.7368	10	1.2481	3.3218
			60	2.7348	11	0.4690	2.1032

and inner circle p_2 (overlap ε_{inn}) of the torus by relation (13).

- Specified n number of used rovings to winding of layer. Calculation of optimal m width of rovings by relation (14) and overlap on the inner circle p_2 (overlap ε_{inn}) by relation (13). Overlap ε_{out} on outer circle p_1 is equal $\varepsilon_{out} = 0$ for optimal m width.
- Specified m width of the roving. Calculation of optimal n number of rovings by relation (15) and the overlaps of adjacent rovings on the outer circle p_1 (overlap $\tilde{\varepsilon}_{out}$) and inner circle p_2 (overlap $\tilde{\varepsilon}_{inn}$) by relation (13).

Table 3 contains the calculation of the optimal m width of the roving when the number n of rovings to winding at the desired winding α angle is specified. At the optimal width of m roving, there is zero overlap of adjacent wound rovings on the outer circle p_1 (see Figure 9(a)), and the calculated overlap ε_{inn} on the inner circle p_2 is shown in the table.

Determination of the optimal number \tilde{n} of rovings (by relation (15)) used for a given m width of roving during the winding process on the torus. At the same time, overlap $\tilde{\varepsilon}_{out}$ on the outer circle p_1 and overlap $\tilde{\varepsilon}_{inn}$ on the inner

circle p_2 of the ring torus are calculated in Table 4 by relation (13).

Figure 14 shows the winding of rovings/tape on a ring torus frame corresponding to the fifth row of Table 4.

Example 3 – curved composite frame

The winding of a composite frame composed of two arms connected by a quarter torus is solved in this example. The frame will be wound at an angle $\alpha = +45^\circ$. The optimum number $\tilde{n}_{straight}$ of used rovings on the straight arms of the frame and the optimum number \tilde{n}_{torus} on the curved part are calculated for a fixed width $m = 10$ of used rovings. The calculated optimal values of used rovings are given in Table 5.

All three parts of the frame in Table 5 are wound with the same rovings for the specified winding layer. The optimal number \tilde{n}_{frame} of rovings used to wind the frame is 9, as avoiding gaps is a higher priority than larger overlaps. At the same time, the overlap $\tilde{\varepsilon}_{str_frame}$ of the rovings on the straight parts of the frame and the outer overlap $\tilde{\varepsilon}_{out-frame}$ and inner overlap $\tilde{\varepsilon}_{inn-frame}$ on curved sections of the frame are calculated. Figure 15 shows the winding of a composite frame composed of two arms connected by a quarter torus and with the parameters corresponding to Table 5.

Table 5. Determination of optimal number \tilde{n} of used rovings for winding a composite frame composed of two arms connected by a quarter torus.

Input parameters

Major radius of frame torus part $R = 102$ [mm]

Minor radius of the frame torus part and radius of the straight part of the frame $r = 18$ [mm]

Width of used rovings $m = 10$ [mm]

Winding angle $\alpha = 45^\circ$

Auxiliary calculation

Parameter of torus $\omega = 5,6666$

Output parameters

Frame straight part – optimal number of rovings $\tilde{n}_{\text{straight}} = 8$,
overlap $\tilde{\epsilon}_{\text{straight}} = 0,0034$ [mm]

Frame torus part – optimal number of rovings $\tilde{n}_{\text{torus}} = 9$
overlap $\tilde{\epsilon}_{\text{inn}} = 2.3657$ [mm], overlap $\tilde{\epsilon}_{\text{out}} = 0.6562$ [mm],

Overall optimum

Overall optimal number of rovings $\tilde{n}_{\text{frame}} = \tilde{n}_{\text{torus}} = 9$;

overlap $\tilde{\epsilon}_{\text{str_frame}} = 1.1141$ [mm],

overlap $\tilde{\epsilon}_{\text{inn_frame}} = \tilde{\epsilon}_{\text{inn}} = 2.3657$ [mm],

overlap $\tilde{\epsilon}_{\text{out_frame}} = \tilde{\epsilon}_{\text{out}} = 0.6562$ [mm]

Note 9

The zero overlaps of adjacent rovings are usually considered using the relations in Chapter 2 (especially relations (4) and (13)). In practice, it is possible to consider the roving width $m-1$ [mm] instead of m [mm] and thus require an overlap of 1 [mm] instead of zero overlap.

Note 10

The verification/validation of the correct winding of the rovings in the examples in this chapter can be done as follows. The correctness of the winding angle α for a straight frame can be determined by measuring the pitch v of the helix formed by the axis of the wound roving h_R while knowing the radius r of the wound frame (see Figure 6(a), $\tan \alpha = v / 2\pi r$). Similarly, two adjacent rovings can be wound only and measure their overlaps or gaps between them and verify the measurements with calculations using relations (4), (6) for a straight frame, or using relations (13), (15) for a frame section forming part of a torus.

Conclusion

The fabrication technology of a specific type of polymer composite frame by winding of fibers is based on the experience of specialists in composite materials and the outputs of the software modeling tools used. The mathematical modeling of the loading of the composite frame determines the geometric shape of the composite, the number of wound layers formed by the fiber reinforcement, and their material composition. The usual materials based on fibers

are carbon, glass, and aramid rovings, or their combination. When combining materials, rovings made from recycled materials are also increasingly used. The outputs of modeling also include the required winding angles of the individual winding layers depending on the load on the composite frame.

However, some output requirements may be difficult to meet in the practical process of fabrication of a composite frame. Compliance with the required winding angles can be difficult with more complicated frame geometry. Similarly, achieving windings without gaps and large overlaps of adjacent rovings is difficult, especially for curved frame parts. If the curved frame section forms part of the ring torus and the aspect ratio of the corresponding torus is large, the winding is complicated.

The theoretical outputs of the paper can be the basis for the initial design of composite reinforcement (material and type of roving) for layer winding. With a fixed number of rovings (determined by the number of coils on the rotating ring of the winding head), the optimum width of the fiber roving can be determined. Similarly, for a given number of rovings used in winding the fiber layer, the optimum width of the rovings used can be calculated. For a desired winding angle, a specific roving width, and a number of rovings, the mathematical relationships presented in this article can be used to determine exactly whether a gap or overlap will form when two adjacent rovings are wound and calculate its size. Calculations can be performed for frames containing straight sections and sections forming a ring torus part. The calculation procedure allows for avoiding the trial-and-error method, and based on the technological, design, and material inputs, a qualitatively homogeneous fiber reinforcement/layer for the future composite part can be obtained.

Declaration of conflicting interests

The author(s) declared no potential conflicts of interest with respect to the research, authorship, and/or publication of this article.

Funding

The author(s) disclosed receipt of the following financial support for the research, authorship, and/or publication of this article: This article was supported by the project “Modular platform for autonomous chassis of specialized electric vehicles for freight and equipment transportation,” Reg. No. CZ.02.1.01/0.0/0.0/16_025/0007293, Technical University of Liberec (TUL). Also, the authors appreciate the support of Chair of Composite Materials and Technical Mechanics, Faculty of Mechanical Engineering, Universität der Bundeswehr München (UniBW) through the project “Development of Concept and Materials for a Space-adapted Hydrogen Tank for Efficient Integration in Aircraft,” under the guidance of German Aerospace Center (DLR), which is financed by the “Bundesministerium für Wirtschaft und Klimaschutz” – registration number 20E2204C.

The financial support by Universität der Bundeswehr München for Open Access publication is also acknowledged.

ORCID iDs

Jaroslav Mlýnek  <https://orcid.org/0000-0002-3386-6738>

Seyed Saeid Rahimian Koloor  <https://orcid.org/0000-0002-1820-6379>

Martina Ryvolová  <https://orcid.org/0000-0003-2080-1473>

Tobias Dickhut  <https://orcid.org/0000-0003-3633-1058>

References

- Mlýnek J, Petrů M, Martinec T, et al. Fabrication of high-quality polymer composite frame by a new method of fiber winding process. *Polymers* 2020; 12(5): 1037.
- Gay D. *Composite materials: design and applications*. Boca Raton: CRC Press, 2022.
- Sharma S, Sowtharya L and Kar KK. Polymer-based composite structures: processing and applications. In: Kar KK (ed.) *Composite materials: processing, applications, characterizations*. Berlin, Heidelberg: Springer. 2017, pp.1–36.
- Mlýnek J, Rahimian Koloor SS, Martinec T, et al. Fabrication of high-quality straight-line polymer composite frame with different radius parts using fiber winding process. *Polymers* 2021; 13(4): 497.
- Mlýnek J, Petrů M and Martinec T. Design of composite frames used in agricultural machinery. In: *Proceedings of the 7th TAE*, 2019.
- Koroteeva LI, Sharonov AV, Astakhov PA, et al. The design of composite materials of prescribed structure and properties. *Int Polym Sci Technol* 2017; 44(7): 17–20.
- Wong KJ, Johar M, Koloor SSR, et al. Moisture absorption effects on mode II delamination of carbon/epoxy composites. *Polymers* 2020; 12(9): 2162.
- Koloor RSS, Karimzadeh A, Abdullah MR, et al. Linear-nonlinear stiffness responses of carbon fiber-reinforced polymer composite materials and structures: A numerical study. *Polymers* 2021; 13(3): 344.
- Shi K, Hu D, Li D, et al. Sound absorption behaviors of composite functionally graded acoustic structure under hydrostatic pressure. *Appl Acoust* 2023; 211: 109474.
- Hamidinejad M, Salari M, Ma L, et al. Electrically and thermally graded microcellular polymer/graphene nanoplatelet composite foams and their EMI shielding properties. *Carbon N Y* 2022; 187: 153–164.
- Wang X, Wang C, Chu C, et al. Structure-function integrated biodegradable Mg/polymer composites: design, manufacturing, properties, and biomedical applications. *Bioact Mater* 2024; 39: 74–105.
- Alizadeh-Osgouei M, Li Y and Wen C. A comprehensive review of biodegradable synthetic polymer-ceramic composites and their manufacture for biomedical applications. *Bioact Mater* 2019; 4(1): 22–36.
- Shah IA, Khan R, Koloor SSR, et al. Finite element analysis of the ballistic impact on auxetic sandwich composite human body armor. *Materials* 2022; 15(6): 2064.
- Abdi B, Koloor SSR, Abdullah MR, et al. Effect of strain-rate on flexural behavior of composite sandwich panel. *Appl Mech Mater* 2012; 229: 766–770.
- Kumar S, Singh I R, Koloor SS, et al. On laminated object manufactured FDM-printed ABS/TPU multimaterial specimens: an insight into mechanical and morphological characteristics. *Polymers* 2022; 14(19): 4066.
- Farokhi Nejad A, Rahimian Koloor SS, Syed Hamzah SMSA, et al. Mechanical behaviour of pin-reinforced foam core sandwich panels subjected to low impact loading. *Polymers* 2021; 13(21): 3627.
- Joshani M, Koloor SSR and Abdullah R. Damage mechanics model for fracture process of steel-concrete composite slabs. *Appl Mech Mater* 2012; 165: 339–345.
- Khan MS, Abdul-Latif A, Koloor SSR, et al. Representative cell analysis for damage-based failure model of polymer hexagonal honeycomb structure under the out-of-plane loadings. *Polymers* 2020; 13(1): 52.
- Koloor SSR, Abdul-Latif A and Tamin MN. Mechanics of composite delamination under flexural loading. *Key Eng Mater* 2011; 462: 726–731.
- Öztürk Brönnimann R and Modregger P. Defect detection in glass fabric reinforced thermoplastics by laboratory-based X-ray scattering. *Compos B Eng* 2023; 252: 110502.
- He Y, Li Y, Ju K, et al. Elastomeric microfluidic valve for active resin flow control within composite structure. *Compos Struct* 2020; 254: 112844.
- Kim C, Teng H, Tucker CL, et al. The continuous curing process for thermoset polymer composites. Part 1: modeling and demonstration. *J Compos Mater* 1995; 29(9): 1222–1253.
- Rajak DK, Wagh PH and Linul E. Manufacturing technologies of carbon/glass fiber-reinforced polymer composites and their properties: a review. *Polymers* 2021; 13(21): 3721.
- Jayasekara D, Lai NYG, Wong KH, et al. Level of automation (LOA) in aerospace composite manufacturing: present status and future directions towards industry 4.0. *J Manuf Syst* 2022; 62: 44–61.
- Loeliger A, Yang E and Bomphray I. *An overview of automated manufacturing for composite materials*. In: *2021 26th International conference on automation and computing (ICAC)*, 2021. New York: IEEE.
- Kassapoglou C. *Design and analysis of composite structures: with applications to aerospace structures*. Chichester: John Wiley & Sons, 2013.
- McIlhagger A, Archer E and McIlhagger R. Manufacturing processes for composite materials and components for aerospace applications. In: *Polymer composites in the aerospace industry*, Newtownabbey, Ulster: Ulster University 2020, pp.59–81.
- Vargas Rojas E, Chapelle D, Perreux D, et al. Unified approach of filament winding applied to complex shape mandrels. *Compos Struct* 2014; 116: 805–813.
- Quanjin M, Rejab MRM, Idris MS, et al. Design and optimize of 3-axis filament winding machine. *IOPIOP Conf Ser Mater Sci Eng* 2017; 257: 012039.
- Quanjin M, Rejab MRM, Idris MS, et al. Filament winding technique: SWOT analysis and applied favorable factors. *J Mech Eng* 2019; 3(1): 1–25.
- Peters ST. *Composite filament winding*. ASM International, 2011.
- Srivastava S and Hoda S. A brief theory on latest trend of filament winding machine. *Int J Adv Eng Res Sci* 2016; 3(4): 258859.

33. Zu L, Koussios S and Beukers A. Design of filament-wound circular toroidal hydrogen storage vessels based on non-geodesic fiber trajectories. *Int J Hydrogen Energy* 2010; 35(2): 660–670.
34. Laval C. CADWIND 2006–20 years of filament winding experience. *Reinforced Plast* 2006; 50(2): 34–37.
35. Skinner ML. Trends, advances and innovations in filament winding. *Reinforced Plast* 2006; 50(2): 28–33.
36. Li H, Ma Y and Li M. Computer aided path design for filament winding torus. *J Reinforced Plast Compos* 2022; 41(21-22): 861–869.
37. Kyosev Y. *Advances in braiding technology: specialized techniques and applications*. Woodhead Publishing, 2016.
38. Bilisik K, Karaduman NS and Bilisik NE. Applications of braided structures in transportation. In: Rana S and Figueiro R (ed.) *Braided structures and composites: production, properties, mechanics and technical applications*. Boca Raton, FL: Taylor and Francis, 2015, pp. 255–295.
39. Minsch N, Herrmann FH, Gereke T, et al. Analysis of filament winding processes and potential equipment technologies. *Procedia CIRP* 2017; 66: 125–130.
40. Sofi T, Neunkirchen S and Schledjewski R. Path calculation, technology and opportunities in dry fiber winding: a review. *Adv Manuf Polym Compos Sci* 2018; 4(3): 57–72.
41. Sofi TR and Schledjewski R. Winding trajectories for dry filament wound preforms. In: *18th European Conference of Composite Materials (ECCM18)*, Athen, Greece 2018.
42. Martinec T, Mlýnek J and Petrů M. Calculation of the robot trajectory for the optimum directional orientation of fibre placement in the manufacture of composite profile frames. *Robot Comput Integr Manuf* 2015; 35: 42–54.
43. Shifrin T. *Differential geometry: a first course in curves and surfaces*. Athens: University of Georgia, 2015, p.24.
44. Mlýnek J, Petrů M, Ryvolová M, et al. Winding optimization of composite frame by dry fiber rovings. *J Ind Text* 2022; 52: 15280837221114639.
45. Do Carmo MP. *Differential geometry of curves and surfaces: revised and updated second edition*. Rio de Janeiro: Courier Dover Publications, 2016.
46. Olsen K and Bohr J. Geometry of the toroidal N-helix: optimal-packing and zero-twist. *New J Phys* 2012; 14(2): 023063.
47. Mlýnek J, Rahimian Koloor SS and Knobloch R. Optimal roving winding on toroidal parts of composite frames. *Polymers* 2023; 15(15): 3227.
48. Benenson W, Harris JW, Stöcker H, et al. *Handbook of Physics*. New York: Springer, 2006.
49. Oromiehie E, Prusty BG, Compston P, et al. Automated fibre placement based composite structures: review on the defects, impacts and inspections techniques. *Compos Struct* 2019; 224: 110987.